

# Exchange-bias controlled correlations in magnetically encapsulated twisted van der Waals dichalcogenides

D. Soriano<sup>1</sup> and J. L. Lado<sup>2</sup>

<sup>1</sup>*Radboud University, Institute for Molecules and Materials, NL-6525 AJ Nijmegen, the Netherlands*

<sup>2</sup>*Department of Applied Physics, Aalto University, 00076 Aalto, Espoo, Finland*

(Dated: March 24, 2022)

Twisted van der Waals materials have become a paradigmatic platform to realize exotic correlated states of matter. Here, we show that a twisted dichalcogenide bilayer (WSe<sub>2</sub>) encapsulated between a magnetic van der Waals material (CrBr<sub>3</sub>) features flat bands with tunable valley and spin flavors. We demonstrate that, when electron-electron interactions are included, spin-ferromagnetic and valley-ferromagnetic states emerge in the flat bands, stemming from the interplay between correlations, intrinsic spin-orbit coupling and exchange proximity effects. We show that the specific symmetry broken state is controlled by the relative alignment of the magnetization of the encapsulation, demonstrating the emergence of correlated states controlled by exchange bias. Our results put forward a new van der Waals heterostructure where symmetry broken states emerge from a genuine interplay between twist engineering, spin-orbit coupling and exchange proximity, providing a powerful starting point to explore exotic collective states of matter.

## I. INTRODUCTION

Two-dimensional materials have risen as a paradigmatic platform to engineer emergent states of matter. This flexibility stems from the capability of stacking different two-dimensional materials on top of each other, allowing to combine electronic orders. Among the different two-dimensional materials, transition metal dichalcogenides<sup>1–6</sup> attracted much attention due to their strong spin orbit-coupling effects. This has allowed exploiting different early proposals in spintronics such as spin-charge conversion<sup>7</sup> valley control,<sup>8–11</sup> and optically generated spin currents,<sup>12,13</sup> demonstrating the possibilities for magnetic control in two-dimensional materials. In this line, the recent discovery, and isolation of two-dimensional magnetic materials<sup>14–20</sup> has allowed pushing this idea even further, providing a purely van der Waals platform for spintronic physics.

Moire structures are known to emerge in generic twisted two dimensional materials, including graphene,<sup>21,22</sup> transition metal dichalcogenides (TMDC),<sup>23–28</sup> boron nitride,<sup>29</sup> MoO<sub>3</sub><sup>30</sup> and ferromagnets.<sup>31</sup> In particular, twisted transition metal dichalcogenide systems provide unique opportunities for spintronics, due to the strong spin-orbit coupling.<sup>8,32–37</sup> Correlated states in twisted dichalcogenides materials have been also demonstrated, stemming from the emergence of quasi-flat bands.<sup>23,24,38–51</sup> Importantly, the strong spin-orbit effects, together with the emergent valley and layer degrees of freedom, bring forward a whole new set of possibilities<sup>3,36,37,52</sup> for engineering strongly correlated states of matter in twisted dichalcogenides. In particular, the spin-valley locking<sup>53,54</sup> provides a way of controlling the internal quantum numbers of a symmetry broken state.

Here we show that a correlated state controlled by exchange bias can be engineered in a van der Waals heterostructure made of magnetic two-dimensional materi-

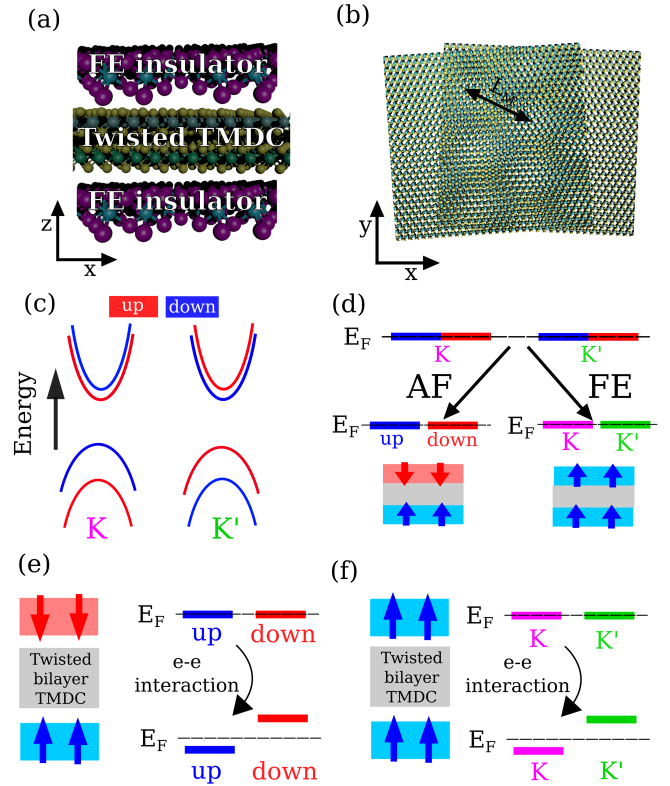


FIG. 1. Sketch of the van der Waals exchanged dichalcogenide multilayer (a) and sketch of the emergence of moire superlattice (b). Panel (c) shows a sketch of the typical band structure of TMDC when spin-orbit coupling effects are considered. Panel (d) shows the possible lifting of degeneracies that the magnetic encapsulation can create. Panel (e,f) shows the interaction-induced symmetry breaking of the low energy states. For antiferromagnetic alignment (e) spin symmetry broken state appears, whereas for ferromagnetic alignment (f) a valley symmetry broken state emerges.

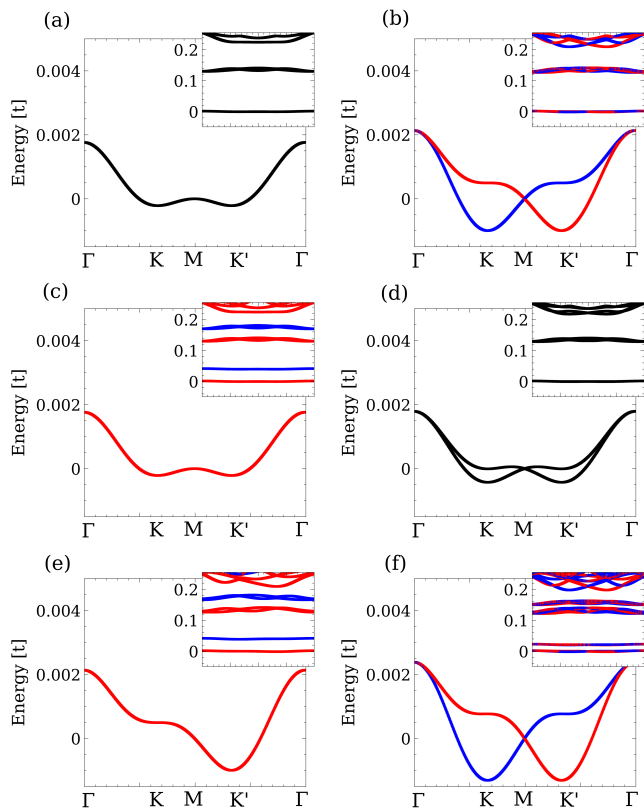


FIG. 2. Band structure of a twisted dichalcogenide with a twist angle of  $1.8^\circ$  in the absence of exchange effects (a,b), with zero SOC (a) and with finite SOC (b). Panels (c,d) shows the bandstructure in the absence of SOC, but with a finite exchange bias, having a ferromagnetic alignment between the layers in (c) and antiferromagnetic in (d) Panels (e,f) show the band structures with finite SOC and exchange fields, having a ferromagnetic alignment between the layers in (e) and antiferromagnetic in (f). In the cases (e,f), the low energy states are formed by two bands, yet with dramatically different orbital content as sketched in Fig. 1d.

als and a twisted dichalcogenide bilayer. In particular, we demonstrate that a magnetic exchange bias can control the symmetry broken state of twisted dichalcogenide system, creating a transition from valley ferromagnetism to spin ferromagnetism. Our results put forward exchange bias as a powerful knob to control symmetry broken states in magnetically encapsulated twisted dichalcogenide materials. The manuscript is organized as follows. In Section II we show the emergence of nearly flat bands controlled by spin-orbit coupling and exchange coupling in the magnetically encapsulated multilayer. In Section III we show the selective switching between interaction-induced valley ferromagnetism and spin ferromagnetism by controlling the magnetization of the encapsulation. In Section IV we estimate the strength of the effective exchange fields by means of first-principles calculations for a specific  $\text{CrBr}_3/\text{WSe}_2$  based structure. Finally, in Section III we summarize our conclusions.

## II. CONTROLLING FLAT BANDS WITH EXCHANGE BIAS

We first address the emergence of flat bands in the magnetic van der Waals heterostructure, and in particular how spin-orbit and exchange effects the low energy flat bands. In the following, we consider an effective model for a transition metal dichalcogenide in a honeycomb lattice, that captures in an effective fashion the low energy valence and conduction bands. For the sake of concreteness, we will focus on the physics emerging in the valence band of the model. We will consider a twisted van der Waals dichalcogenide, encapsulated between a ferromagnetic insulator, where we have integrated out the degrees of freedom of the ferromagnetic insulator. The total Hamiltonian is of the form

$$H = H_0 + H_{SOC} + H_J \quad (1)$$

with  $H_0$  the non-relativistic Hamiltonian,  $H_{SOC}$  the spin-orbit coupling correction and  $H_J = H_{AF}/H_{FE}$  the exchange proximity effect

$$H_0 = \sum_{\langle ij \rangle} t c_{i,s}^\dagger c_{j,s} + m \sum_{i,s} \vartheta_{ii}^z c_{i,s}^\dagger c_{i,s} + \sum_{i,j,s} t^\perp(\mathbf{r}_i, \mathbf{r}_j) c_{i,s}^\dagger c_{j,s} \quad (2)$$

$$H_{SOC} = i\lambda_{SOC} \sum_{\langle\langle ij \rangle\rangle, s, s'} \nu_{ij} \sigma_{s,s'}^z c_{i,s}^\dagger c_{j,s'} \quad (3)$$

$$H_{AF} = J_{AF} \sum_{i,s,s'} \tau_i \sigma_{s,s'}^z c_{i,s}^\dagger c_{i,s'} \quad (4)$$

$$H_{FE} = J_{FE} \sum_{i,s,s'} \sigma_{s,s'}^z c_{i,s}^\dagger c_{i,s'} \quad (5)$$

where  $t$  is a first neighbor hopping,  $t^\perp(\mathbf{r}_i, \mathbf{r}_j)$  parametrize the interlayer coupling,<sup>55–57</sup>  $\vartheta_{ii}^z$  is the sublattice Pauli matrix,  $m$  denotes the onsite energy imbalance between the two sites of the honeycomb lattice,  $\sigma_{s,s'}^z$  is the spin Pauli matrix,  $\nu_{ij} = \pm 1$  for clock-wise/anti-clockwise hopping,<sup>58</sup>  $\langle \rangle$  denotes sum over first neighbors in a layer,  $\langle\langle \rangle\rangle$  denotes sum over second neighbors in a layer, and  $\tau_i = \pm 1$  for upper/lower layer. The previous model applied for a single layer faithfully captures the electronic structure at the  $K$  and  $K'$  points,<sup>54,59,60</sup> and therefore can be used as a starting point for flat bands stemming from the dichalcogenide valleys. We note that more sophisticated models for a dichalcogenide could be considered, yet for the sake of simplicity we here focus on the minimal one that captures the spin-valley physics at the valleys.

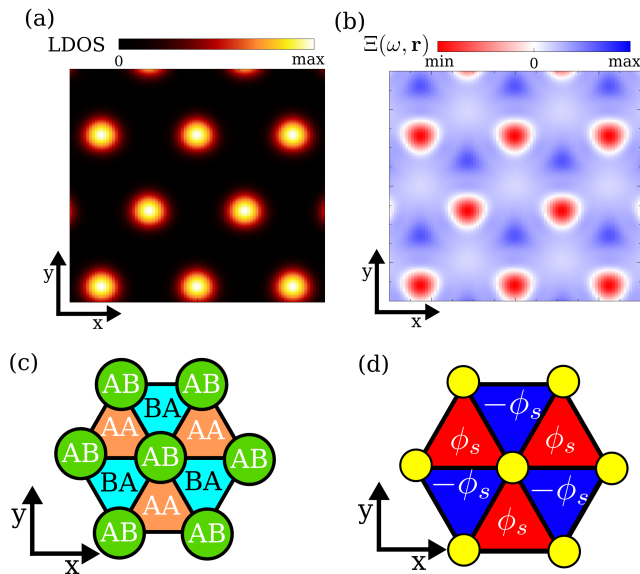


FIG. 3. Local density of states of the lowest flat band, showing the emergence of localized states in a triangular lattice. Focusing now in the heterostructure with antiferromagnetic alignment of Fig. 2f, panel (b) shows the real space spin flux at  $\omega = \epsilon_F$ , showing the emergence of non-trivial spin topology. Panel (c) shows the sketch of the different parts of the superlattice, and panel (d) a low energy model for the nearly flat bands.

With the previous effective model, we now compute the electronic structure of the magnetically encapsulated dichalcogenide multilayer. In particular, it is interesting to look in detail at the degeneracy of the low energy manifold in different regimes. Let us start with the case  $J_{AF} = J_{FE} = \lambda_{SOC} = 0$ , the case in which both exchange and spin-orbit coupling effects are neglected. As shown in Fig. 2a the band structure for a structure with a twist angle  $1.8^\circ$  shows nearly flat bands as expected from twisted dichalcogenide systems. It is important to note that such energy bands are four-fold degenerate, two times from valley, and two times due to spin. Such phenomenology is analogous to twisted graphene multilayers or twisted boron nitride. Due to the existence of such degeneracy, it is expected that the addition of additional terms breaking that symmetry will create splittings between the different sectors. When we consider the effect of intrinsic spin-orbit coupling ( $\lambda_{SOC} = 0.02t$ ) as shown in Fig. 2b a momentum-dependent spin splitting appears, yet the valley degeneracy remains along the shown  $k$ -path. As a result, the low energy manifold remains four-fold degenerate. It is interesting to note that the inclusion of spin-orbit coupling slightly increases the bandwidth of the low energy bands, yet still keeping an overall small bandwidth. Besides the splitting created in the low energy bands, additional splittings are created at higher energies.

Let us now focus in the cases hosting only exchange fields, and in the absence of spin-orbit coupling. The

simplest case to consider is to the ferromagnetic configuration ( $J_{FE} = 0.02t$ ), in which the spin degeneracy is lifted Fig. 2c. In this situation, a uniform shift between up and down channels take place, and the low energy bands become just two-fold degenerate due to valley degeneracy. A more interesting scenario happens for antiferromagnetic exchange bias ( $J_{AF} = 0.05t$ ) Fig. 2d, in which a small splitting appears in the bands, yet without fully lifting the degeneracy of the low energy manifold. It is especially interesting to note that the band structure with spin-orbit coupling (Fig. 2b) and antiferromagnetic exchange bias (Fig. 2d) both show a four-fold degeneracy of the low energy manifold, in contrast with the trivial lifting of degeneracy created by the ferromagnetic exchange field (Fig. 2c).

We now move on to the case when both exchange fields and spin-orbit coupling are non-zero. We start with the case of ferromagnetic exchange ( $J_{FE} = 0.02t$ ) and non-zero SOC ( $\lambda_{SOC} = 0.02t$ ), shown in Fig. 2e. The low energy manifold is still two-fold degenerate stemming from the valley degree of freedom (both bands are superimposed in Fig. 2e), yet with a clear asymmetry between  $-k$  and  $+k$  due to the combination of SOC effect and exchange field. A more interesting scenario corresponds to the antiferromagnetic exchanged case ( $J_{AF} = 0.02t$ ) with non-zero SOC ( $\lambda_{SOC} = 0.02t$ ) shown in Fig. 2f. It is clearly observed that now the low energy manifold is two-fold degenerate, in contrast with Figs. 2bd (see the splitting showed in the insets). The low energy degeneracy comes from a combination of time-reversal and mirror symmetries, and could be lifted with an electric field between the layers. It is worth to remark that in both cases, ferromagnetic and antiferromagnetic bias, the low energy manifold is two-fold degenerate, yet with dramatically different quantum numbers. This feature will be important when considering the effect of electronic interactions.

Before moving on to interaction effects, it is interesting to understand the nature of the low energy states (Fig. 3abcd). The states associated to the two low energy flat bands form an emergent triangular lattice, as shown in the local density of states of (Fig. 3a). This is of course already suggested by the band structures of Fig. 2, that features the typical dispersion of a triangular lattice. Interestingly, the location of this emergent triangular superlattice corresponds to regions of the twisted system showing AB stacking (Fig. 3c), namely a region where one of the atoms fall in the hollow site, in strike contrast with the conventional AA localization in twisted graphene bilayers.<sup>55,61,62</sup> This is easily rationalized by taking into account that, whereas for graphene AB and BA regions are equivalent, in a twisted dichalcogenide bilayer AB corresponds to Mo-Mo stacking, whereas BA corresponds to S-S stacking, and therefore are inequivalent. As a result, a triangular arrangement of the states in the AB regions becomes possible.

The triangular arrangement between the states, together with the low energy dispersion, suggests that

this system can be described with a low energy effective model. To gain insight into this, it is interesting to look at the valley spin flux<sup>63–66</sup> in the moire unit cell defined as

$$\Xi(\mathbf{r}, \omega) = \int \frac{d^2\mathbf{k}}{(2\pi)^2} \frac{\epsilon_{\alpha\beta}}{2} \langle \mathbf{r} | \mathcal{G}(\partial_{k_\alpha} \mathcal{G}^{-1})(\partial_{k_\beta} \mathcal{G}) | \mathbf{r} \rangle. \quad (6)$$

where  $\mathcal{G}$  is the valley-spin Green's function defined as

$$\mathcal{G}(\omega) = [\omega - H(\mathbf{k}) + i0^+]^{-1} \mathcal{V}_z S_z \quad (7)$$

with  $\mathcal{V}_z$  the valley operator,<sup>64,66–69</sup>  $S_z$  the spin operator and  $H(\mathbf{k})$  the Bloch Hamiltonian.

The valley-spin Chern number  $\mathcal{C}$  can be computed as  $\mathcal{C} = \int_{-\infty}^0 d\omega \int d^2\mathbf{r} \Xi(\mathbf{r}, \omega)$ , and as result  $\Xi(\mathbf{r}, \omega)$  the real space energy resolved valley-spin flux.<sup>63–66</sup> The valley operator  $\mathcal{V}_z$  is defined in the tight binding basis as<sup>64,66–69</sup>

$$\mathcal{V}_z = \frac{i}{3\sqrt{3}} \sum_{\langle\langle ij \rangle\rangle, s} \vartheta_{ij}^z \nu_{ij} c_{i,s}^\dagger c_{j,s} \quad (8)$$

where  $\nu_{ij} = \pm 1$  for clock-wise/anticlock-wise hopping,  $\langle\langle \rangle\rangle$  denotes sum over second neighbors in a layer, and  $\vartheta_{ij}^z$  is the sublattice Pauli matrix. The previous operator takes the eigenvalues  $\pm 1$  at the microscopic  $K$  and  $K'$ , and as a result can be used to compute the valley flavor of an eigenstate. it is worth to note that this operator will be especially useful in the next section when computing valley symmetry breaking in the real tight binding model.

Focusing on the case with antiferromagnetic configuration, we observe that real space valley fluxes at the Fermi energy  $\omega = \epsilon_F$  emerge in the unit cell (Fig. 3b), similarly to other van der Waals multilayers.<sup>64–66</sup> The combination of triangular arrangement (Fig. 3a) and real space valley-spin flux (Fig. 3b) suggest that the low energy band structure can be captured with an effective triangular lattice with spin-valley fluxes  $H = \sum_{\langle ij \rangle, s, s'} e^{i\sigma_{s,s'}^z \varphi_{ij}} d_{i,s}^\dagger d_{j,s'}$ , where  $d_{i,s}^\dagger, d_{i,s}$  are the creation/annihilation operators for the Wannier states,  $\varphi_{ij}$  are the phases associated to the real space flux of the supercell  $\phi_S$  (Fig. 3d). This low energy Wannier model would allow to study interaction effects without having to perform a calculation for the whole moire unit cell, and similar models have been explored in a variety of twisted two dimensional materials.<sup>47,65,70</sup> The form of the effective interactions in these low energy models can be non-trivial, due to the potentially extended nature of the Wannier states.<sup>71,72</sup> Here, in order to perform unbiased calculations, we will explore interaction effects with the full microscopic model including onsite, first and second neighbor interactions.

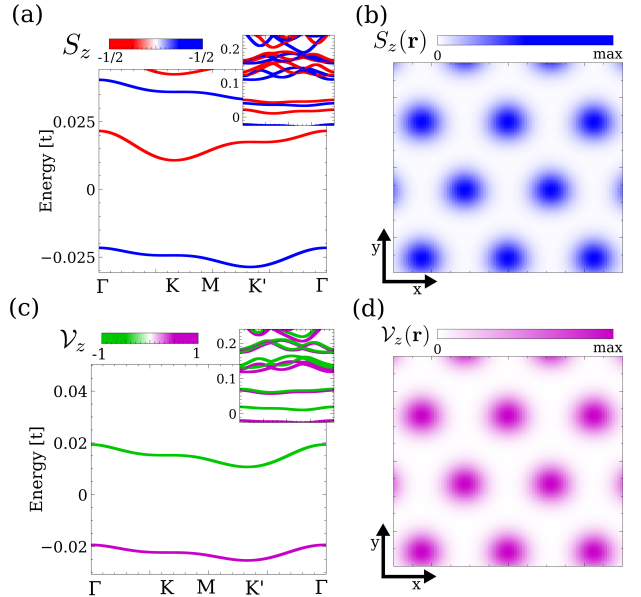


FIG. 4. Selfconsistent electronic structure with an antiferromagnetic alignment between the leads (a,b), and with a ferromagnetic one (c,d). In the case of an antiferromagnetic alignment (a,b), interactions give rise to a spin polarized ground state (a), with a net  $S = 1/2$  magnetic moment per unit cell (b). In the case of ferromagnetic alignment (c,d), interactions give rise to a valley polarized ground state (c), with a net valley moment per unit cell (d).

### III. INTERACTION-INDUCED SYMMETRY BREAKING IN EXCHANGED-BIAS FLAT BANDS

We now focus on the effect of interactions in the full real space model. For that purpose, we consider a generic interacting Hamiltonian with interactions up to second neighbors of the form

$$H_I = H_I^{(0)} + H_I^{(1)} + H_I^{(2)} \quad (9)$$

where  $H_I^{(0)}$  is the local Hubbard interaction with strength  $U$

$$H_I^{(0)} = U \sum_i c_{i,\uparrow}^\dagger c_{i,\uparrow} c_{i,\downarrow}^\dagger c_{i,\downarrow} \quad (10)$$

$H_I^{(1)}$  is the first neighbor interaction with strength  $V_1$

$$H_I^{(1)} = V_1 \sum_{\langle ij \rangle} \left[ \left( \sum_s c_{i,s}^\dagger c_{i,s} \right) \left( \sum_s c_{j,s}^\dagger c_{j,s} \right) \right] \quad (11)$$

$H_I^{(2)}$  is the second neighbor interaction with strength

$V_2$

$$H_I^{(2)} = V_2 \sum_{\langle\langle ij \rangle\rangle} \left[ \left( \sum_s c_{i,s}^\dagger c_{i,s} \right) \left( \sum_s c_{j,s}^\dagger c_{j,s} \right) \right] \quad (12)$$

We note that by construction, the interaction Hamiltonian is SU(2) symmetric. We decouple the previous Hamiltonian with a conventional non-collinear mean-field approximation, which we solve selfconsistently. In the following we take  $U = 2t$ ,  $V_1 = 1.5t$  and  $V_2 = 0.5t$ , and we will focus on the the of a single electron per moire unit cell, that turns the low energy flat bands half filled. We note that the same results are expected for a single hole per unit cell and, as it will be shown later, this would be physically achievable regime for the WSe<sub>2</sub>/CrBr<sub>3</sub> twisted multilayer.

We now consider the two different scenarios for the magnetic encapsulation, the heterostructure with with antiferromagnetic configuration (Fig. 4ab), and with ferromagnetic configuration (Fig. 4cd). As elaborated above, depending on the configuration of the magnetic electrodes, the spin or valley degeneracy is lifted. In the low energy manifold, which is now just two fold degenerate, interactions can give rise to an additional symmetry breaking.

We focus first on the case with antiferromagnetic configuration, whose low energy manifold has two bands, one per spin channel (Fig. 2f). Due to this spin degeneracy, correlation effects could be able to lift the degeneracy and open up a gap, as we explicitly show below. We now take the interaction terms introduced in Eqs. 101112, and solve the selfconsistent mean field equations. We obtain that, upon introducing interactions, symmetry broken state emerges, hosting a net spin magnetic moment per supercell and lifting the degeneracy of the low energy band structure.<sup>73</sup> The mean field band structure shown in Fig. 4a shows that a spontaneous exchange splitting appears in the band structure, lifting the degeneracy of the low energy manifold introduced in Fig. 2f. The projection in real space of the spin operator  $S_z(\mathbf{r})$  shows that, associated with the lifting of degeneracy, a non-zero magnetic moment emerges, localized in the regions with AB stacking as shown in Fig. 4b.

We now move on to the case in which the magnetic leads have a ferromagnetic alignment. In this situation, the low energy manifold host two bands, one per valley (Fig. 2e). Given that these two energy band belong to the same spin channel, a magnetic instability cannot lift their degeneracy, in stark contrast with the antiferromagnetic encapsulation. Upon introducing electronic interactions of Eqs. 101112 and solving the selfconsistent problem, we obtain a mean field Hamiltonian whose band-structure has an spontaneous interaction induced valley splitting (Fig. 4c). We can compute the expectation value of the valley operator in the unit cell  $\mathcal{V}_z(\mathbf{r})$ , and we observe that a non-zero valley polarization emerges in the regions with AB stacking as shown in Fig. 4d. The

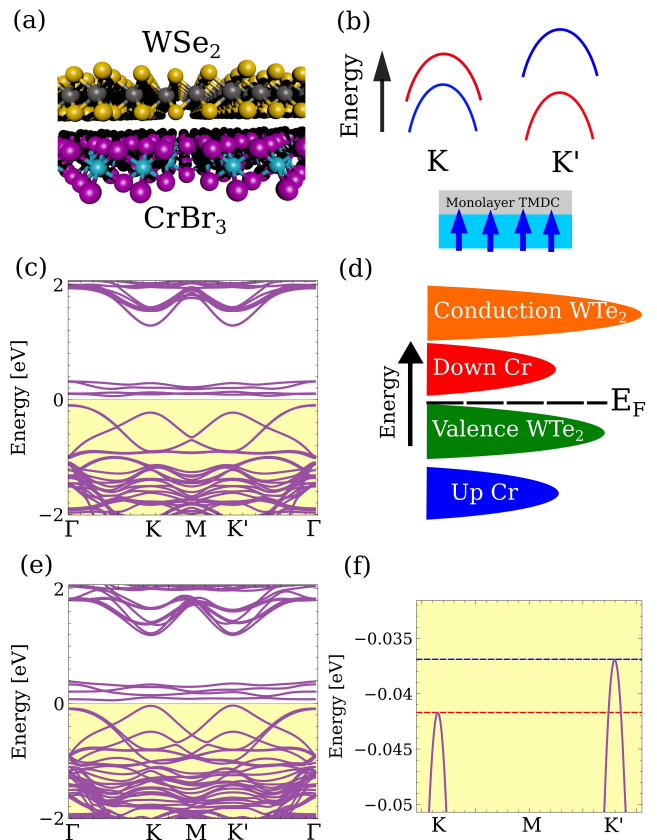


FIG. 5. (a) Sketch of the structure computed from first principles, consisting on WSe<sub>2</sub> on top of CrBr<sub>3</sub>. Panel (b) shows a sketch of the effect of the exchange proximity effect, creating a splitting between the states at K and K'. Panel (c) shows the first principles band-structure of the heterostructure in (a), in the absence of spin-orbit coupling. Panel (d) shows a sketch of the orbitally resolved density of states as obtained in (c). Panel (e) shows the first principles band structure with full non-collinear spin-orbit coupling, and panel (f) shows a zoom on the top of the valence band.

real space expectation value of the valley operator is computed by taking the valley operator of Eq. 8 and adding a localized real space envelope to each site.

The previous calculations demonstrate, using a microscopic interacting model, that the symmetry breaking induced by interactions is controlled by the magnetic alignment of the magnetic substrate. Importantly, the genuine combination of spin-orbit and exchange effects lead to the realization of pure-valley or pure-spin electronic instabilities in the flat bands of twisted dichalcogenides. Finally, it is worth to mention that the previous discussion has focused in a low energy atomistic effective model. In the next section we show using first principles methods, that a specific van der Waals material formed by WSe<sub>2</sub>/CrBr<sub>3</sub> would be described with the effective model considered.

#### IV. FIRST PRINCIPLES CALCULATIONS OF THE $\text{WSe}_2/\text{CrBr}_3$ EXCHANGE BIAS

We finally show via first principles calculations that proximity effect between  $\text{WSe}_2$  and  $\text{CrBr}_3$  leads to an exchange splitting in the valence band of  $\text{WSe}_2$ . The emergence of such splitting can be understood from a second order process in which an electron jumps from the semiconductor to the ferromagnet and back.<sup>74–78</sup> Since the emergence of flat bands in twisted dichalcogenides have already been demonstrated by first principles, here we will focus on the combined effect of exchange proximity effect and spin-orbit coupling. For this sake, we consider a minimal multilayer consisting on  $\text{WSe}_2$  on top of the ferromagnetic insulator  $\text{CrBr}_3$ , as shown in Fig. 5a. In this situation, the exchange proximity effect created by  $\text{CrBr}_3$  on  $\text{WSe}_2$  will give rise to valley splitting in the low energy band-structure, as sketched in Fig. 5b.

We performed our first principles calculations with the all-electron LAPW formalism as implemented in Elk.<sup>79</sup> Correlations in the Cr d-manifold were included with the DFT+U formalism in the Yukawa form,<sup>80</sup> taking  $U = 4$  eV. We first focus on the case without spin-orbit coupling, the resulting band structure is shown in Fig. 5c. The first important feature is that, in the absence of spin-orbit coupling, the top of the valence band is located at  $\Gamma$  instead of  $K$ , and as will be shown later this dramatically changes when spin-orbit coupling is included. Second, it is also worth to note that the conduction band states are formed by unoccupied Cr orbitals, instead of the  $\text{WSe}_2$  states. This orbital arrangement as a function of energy is shown in Fig. 5d. This indicates that for the current van der Waals heterostructure, correlated states in moire flat bands should be searched in the hole-doped regime. Although it is well known that DFT underestimates the Mott gap in correlated magnets, our calculations performed with  $U = 4$  eV for the Cr d-orbitals suggest that they might indeed be located inside the gap in real multilayer. Nevertheless, it must be noted that using a different ferromagnetic insulator such as  $\text{EuS}_2$  may allow to explore the effect of exchange field in conduction electron flat bands.

We now move to consider the heterostructure computed with full non-collinear spin-orbit coupling, whose band structure is shown in Fig. 5e. As anticipated before, in the presence of spin-orbit coupling the top of the valence band is located at  $K$ , in agreement with the low energy model used before. This feature highlights that first principles calculations of flat bands in twisted  $\text{WSe}_2$  can be strongly impacted by the presence of spin orbit coupling, as it dramatically impact the nature of the states at the top of the valence band. In particular we find that, the top of the valence band is 60 meV below the top of the valence band at the  $K/K'$  point. Second, it is observed that the combination of magnetism and spin-orbit coupling breaks the degeneracy between  $k \rightarrow -k$ , giving rise to different dispersion around the  $K$  and  $K'$  points (Fig. 5e). In the present case, we are particularly

interested on its impact at the top of the valence band. Zooming the band structure on the top of the valence band as shown in Fig. 5f, we clearly observe a splitting between the  $K$  and  $K'$  point, which is exactly associated to the combination of exchange proximity effect between  $\text{CrBr}_3$  and  $\text{WSe}_2$  and spin-orbit coupling.<sup>78,81–83</sup> The exchange proximity effect is found on the order of 4 meV, similar to other van der Waals multilayers.<sup>78</sup> The previous first principles results demonstrate both the validity of the low energy model used previous for the top of the valence band, and the possibility of breaking  $K/K'$  via exchange proximity effect, the feature that we used too selectively lift the degeneracy of the flat bands.

We finally note that the previous first principles calculations do not account from additional effects appearing in the twisted system, such as atomic relaxations in the twisted  $\text{WSe}_2$ , rippling between the  $\text{WSe}_2$  and  $\text{CrBr}_3$ , or atomic relaxations in  $\text{CrBr}_3$  stemming from the moire pattern between  $\text{CrBr}_3$  and  $\text{WSe}_2$ . To capture those effects, first principles calculations of a twisted  $\text{CrBr}_3/\text{WSe}_2/\text{WSe}_2/\text{CrBr}_3$  multilayer should be performed, including non-collinear spin-orbit coupling and DFT+U. Nevertheless, given the large unit cells involved, this would be represent a challenging system from the computation point of view.

#### V. CONCLUSIONS

We have shown that a van der Waals heterostructure consisting of twisted dichalcogenide bilayer ( $\text{WSe}_2$ ) encapsulated between two-dimensional ferromagnets ( $\text{CrBr}_3$ ) shows flat bands and correlated states controlled by the magnetic encapsulation. By using an effective atomistic model that incorporates spin-orbit and exchange proximity effects, we showed that such moire system shows flat bands whose internal orbital structure strongly depends on the magnetic encapsulation. Once we include electronic interactions, we demonstrated that depending on the magnetic arrangement, a spontaneous spin-symmetry breaking or valley-symmetry breaking emerges due to correlation effects. Finally, using first-principles calculations, we showed that the proximity between  $\text{CrBr}_3$  and  $\text{WSe}_2$  creates a spin splitting in the  $\text{WSe}_2$ , in agreement with the low energy model used. Our results put forward hybrid magnetic/dichalcogenide twisted multilayers as a versatile platform where spin-orbit and exchange effects drive controllable correlated states.

#### ACKNOWLEDGMENTS

D.S. thanks financial support from EU through the MSCA project Nr. 796795 SOT-2DvdW. J.L.L. acknowledges the computational resources provided by the Aalto Science-IT project. We thank Z. Sun, T. Wolf, G. Blatter, O. Zilberberg, F. Guinea, B. Amorim, M. Sigrist,

M. Roesner and P. Liljeroth for fruitful discussions. Part

of this work was carried out on the Dutch national e-infrastructure with the support of SURF Cooperative

- 
- <sup>1</sup> B. Radisavljevic, A. Radenovic, J. Brivio, V. Giacometti, and A. Kis, *Nature Nanotechnology* **6**, 147 (2011).
- <sup>2</sup> A. Splendiani, L. Sun, Y. Zhang, T. Li, J. Kim, C.-Y. Chim, G. Galli, and F. Wang, *Nano Letters* **10**, 1271 (2010).
- <sup>3</sup> S. Manzeli, D. Ovchinnikov, D. Pasquier, O. V. Yazyev, and A. Kis, *Nature Reviews Materials* **2** (2017), 10.1038/natrevmats.2017.33.
- <sup>4</sup> K. F. Mak, C. Lee, J. Hone, J. Shan, and T. F. Heinz, *Phys. Rev. Lett.* **105**, 136805 (2010).
- <sup>5</sup> R. G. Dickinson and L. Pauling, *Journal of the American Chemical Society* **45**, 1466 (1923).
- <sup>6</sup> J. Wilson and A. Yoffe, *Advances in Physics* **18**, 193 (1969).
- <sup>7</sup> M. Offidani, M. Milletari, R. Raimondi, and A. Ferreira, *Phys. Rev. Lett.* **119**, 196801 (2017).
- <sup>8</sup> H. Zeng, J. Dai, W. Yao, D. Xiao, and X. Cui, *Nature Nanotechnology* **7**, 490 (2012).
- <sup>9</sup> C. K. Safeer, J. Ingla-Aynés, F. Herling, J. H. Garcia, M. Vila, N. Ontoso, M. R. Calvo, S. Roche, L. E. Hueso, and F. Casanova, *Nano Letters* **19**, 1074 (2019).
- <sup>10</sup> Q. Shao, G. Yu, Y.-W. Lan, Y. Shi, M.-Y. Li, C. Zheng, X. Zhu, L.-J. Li, P. K. Amiri, and K. L. Wang, *Nano Letters* **16**, 7514 (2016).
- <sup>11</sup> J. B. S. Mendes, A. Aparecido-Ferreira, J. Holanda, A. Azevedo, and S. M. Rezende, *Applied Physics Letters* **112**, 242407 (2018).
- <sup>12</sup> Y. K. Luo, J. Xu, T. Zhu, G. Wu, E. J. McCormick, W. Zhan, M. R. Neupane, and R. K. Kawakami, *Nano Letters* **17**, 3877 (2017).
- <sup>13</sup> A. Avsar, D. Unuchek, J. Liu, O. L. Sanchez, K. Watanabe, T. Taniguchi, B. Özyilmaz, and A. Kis, *ACS Nano* **11**, 11678 (2017).
- <sup>14</sup> B. Huang, G. Clark, E. Navarro-Moratalla, D. R. Klein, R. Cheng, K. L. Seyler, D. Zhong, E. Schmidgall, M. A. McGuire, D. H. Cobden, W. Yao, D. Xiao, P. Jarillo-Herrero, and X. Xu, *Nature* **546**, 270 (2017).
- <sup>15</sup> M. Gibertini, M. Koperski, A. F. Morpurgo, and K. S. Novoselov, *Nature Nanotechnology* **14**, 408 (2019).
- <sup>16</sup> N. Samarth, *Nature* **546**, 216 (2017).
- <sup>17</sup> C. Gong, L. Li, Z. Li, H. Ji, A. Stern, Y. Xia, T. Cao, W. Bao, C. Wang, Y. Wang, Z. Q. Qiu, R. J. Cava, S. G. Louie, J. Xia, and X. Zhang, *Nature* **546**, 265 (2017).
- <sup>18</sup> M.-W. Lin, H. L. Zhuang, J. Yan, T. Z. Ward, A. A. Puretzky, C. M. Rouleau, Z. Gai, L. Liang, V. Meunier, B. G. Sumpter, P. Ganesh, P. R. C. Kent, D. B. Geohegan, D. G. Mandrus, and K. Xiao, *Journal of Materials Chemistry C* **4**, 315 (2016).
- <sup>19</sup> K. Zhao Du, X. Zhi Wang, Y. Liu, P. Hu, M. I. B. Utama, C. K. Gan, Q. Xiong, and C. Kloc, *ACS Nano* **10**, 1738 (2015).
- <sup>20</sup> C.-T. Kuo, M. Neumann, K. Balamurugan, H. J. Park, S. Kang, H. W. Shiu, J. H. Kang, B. H. Hong, M. Han, T. W. Noh, and J.-G. Park, *Scientific Reports* **6** (2016), 10.1038/srep20904.
- <sup>21</sup> J. M. B. Lopes dos Santos, N. M. R. Peres, and A. H. Castro Neto, *Phys. Rev. B* **86**, 155449 (2012).
- <sup>22</sup> J. M. B. Lopes dos Santos, N. M. R. Peres, and A. H. Castro Neto, *Phys. Rev. Lett.* **99**, 256802 (2007).
- <sup>23</sup> F. Wu, T. Lovorn, E. Tutuc, I. Martin, and A. H. MacDonald, *Phys. Rev. Lett.* **122**, 086402 (2019).
- <sup>24</sup> M. H. Naik and M. Jain, *Phys. Rev. Lett.* **121**, 266401 (2018).
- <sup>25</sup> I. Maity, M. H. Naik, P. K. Maity, H. R. Krishnamurthy, and M. Jain, *Phys. Rev. Research* **2**, 013335 (2020).
- <sup>26</sup> C. H. Lui, Z. Ye, C. Ji, K.-C. Chiu, C.-T. Chou, T. I. Andersen, C. Means-Shively, H. Anderson, J.-M. Wu, T. Kidd, Y.-H. Lee, and R. He, *Phys. Rev. B* **91**, 165403 (2015).
- <sup>27</sup> A. M. Jones, H. Yu, N. J. Ghimire, S. Wu, G. Aivazian, J. S. Ross, B. Zhao, J. Yan, D. G. Mandrus, D. Xiao, W. Yao, and X. Xu, *Nature Nanotechnology* **8**, 634 (2013).
- <sup>28</sup> B. W. H. Baugher, H. O. H. Churchill, Y. Yang, and P. Jarillo-Herrero, *Nature Nanotechnology* **9**, 262 (2014).
- <sup>29</sup> X.-J. Zhao, Y. Yang, D.-B. Zhang, and S.-H. Wei, *Phys. Rev. Lett.* **124**, 086401 (2020).
- <sup>30</sup> M. Chen, X. Lin, T. Dinh, Z. Zheng, J. Shen, Q. Ma, H. Chen, P. Jarillo-Herrero, and S. Dai, arXiv e-prints, arXiv:2004.14588 (2020), arXiv:2004.14588 [cond-mat.mes-hall].
- <sup>31</sup> K. Hejazi, Z.-X. Luo, and L. Balents, *Proceedings of the National Academy of Sciences* **117**, 10721 (2020).
- <sup>32</sup> A. Kormányos, V. Zólyomi, N. D. Drummond, and G. Burkard, *Phys. Rev. X* **4**, 011034 (2014).
- <sup>33</sup> K. F. Mak, K. He, J. Shan, and T. F. Heinz, *Nature Nanotechnology* **7**, 494 (2012).
- <sup>34</sup> T. Cao, G. Wang, W. Han, H. Ye, C. Zhu, J. Shi, Q. Niu, P. Tan, E. Wang, B. Liu, and J. Feng, *Nature Communications* **3** (2012), 10.1038/ncomms1882.
- <sup>35</sup> G. Sallen, L. Bouet, X. Marie, G. Wang, C. R. Zhu, W. P. Han, Y. Lu, P. H. Tan, T. Amand, B. L. Liu, and B. Urbaszek, *Phys. Rev. B* **86**, 081301 (2012).
- <sup>36</sup> X. Xu, W. Yao, D. Xiao, and T. F. Heinz, *Nature Physics* **10**, 343 (2014).
- <sup>37</sup> K. F. Mak and J. Shan, *Nature Photonics* **10**, 216 (2016).
- <sup>38</sup> L. Wang, E.-M. Shih, A. Ghiotto, L. Xian, D. A. Rhodes, C. Tan, M. Claassen, D. M. Kennes, Y. Bai, B. Kim, K. Watanabe, T. Taniguchi, X. Zhu, J. Hone, A. Rubio, A. Pasupathy, and C. R. Dean, arXiv e-prints, arXiv:1910.12147 (2019), arXiv:1910.12147 [cond-mat.mes-hall].
- <sup>39</sup> F. Wu, T. Lovorn, E. Tutuc, and A. H. MacDonald, *Phys. Rev. Lett.* **121**, 026402 (2018).
- <sup>40</sup> M. H. Naik, S. Kundu, I. Maity, and M. Jain, arXiv e-prints, arXiv:1908.10399 (2019), arXiv:1908.10399 [cond-mat.mes-hall].
- <sup>41</sup> J. Wang, Q. Shi, E.-M. Shih, L. Zhou, W. Wu, Y. Bai, D. A. Rhodes, K. Barmak, J. Hone, C. R. Dean, and X. Y. Zhu, arXiv e-prints, arXiv:2001.03812 (2020), arXiv:2001.03812 [cond-mat.mes-hall].
- <sup>42</sup> C. Jin, E. C. Regan, A. Yan, M. I. B. Utama, D. Wang, S. Zhao, Y. Qin, S. Yang, Z. Zheng, S. Shi, K. Watanabe, T. Taniguchi, S. Tongay, A. Zettl, and F. Wang, *Nature* **567**, 76 (2019).

- <sup>43</sup> E. C. Regan, D. Wang, C. Jin, M. I. B. Utama, B. Gao, X. Wei, S. Zhao, W. Zhao, Z. Zhang, K. Yumigeta, M. Blei, J. D. Carlström, K. Watanabe, T. Taniguchi, S. Tongay, M. Crommie, A. Zettl, and F. Wang, *Nature* **579**, 359 (2020).
- <sup>44</sup> Y. Shimazaki, I. Schwartz, K. Watanabe, T. Taniguchi, M. Kroner, and A. Imamoglu, *Nature* **580**, 472 (2020).
- <sup>45</sup> Y. Tang, L. Li, T. Li, Y. Xu, S. Liu, K. Barmak, K. Watanabe, T. Taniguchi, A. H. MacDonald, J. Shan, and K. F. Mak, *Nature* **579**, 353 (2020).
- <sup>46</sup> Y. Zhang, N. F. Q. Yuan, and L. Fu, arXiv e-prints , arXiv:1910.14061 (2019), arXiv:1910.14061 [cond-mat.str-el].
- <sup>47</sup> K. Slagle and L. Fu, arXiv e-prints , arXiv:2003.13690 (2020), arXiv:2003.13690 [cond-mat.str-el].
- <sup>48</sup> Z. Zhan, Y. Zhang, G. Yu, F. G. J. A. Silva-Guillen, and S. Yuan, arXiv e-prints , arXiv:2005.13868 (2020), arXiv:2005.13868 [cond-mat.mes-hall].
- <sup>49</sup> M. Fleischmann, R. Gupta, S. Sharma, and S. Shallcross, arXiv e-prints , arXiv:1901.04679 (2019), arXiv:1901.04679 [cond-mat.mes-hall].
- <sup>50</sup> Z. Zhang, Y. Wang, K. Watanabe, T. Taniguchi, K. Ueno, E. Tutuc, and B. J. LeRoy, arXiv e-prints , arXiv:1910.13068 (2019), arXiv:1910.13068 [cond-mat.str-el].
- <sup>51</sup> Y. Zhang, Z. Zhan, F. Guinea, J. A. Silva-Guillen, and S. Yuan, arXiv e-prints , arXiv:2005.13879 (2020), arXiv:2005.13879 [cond-mat.mes-hall].
- <sup>52</sup> H. M. Hill, A. F. Rigosi, K. T. Rim, G. W. Flynn, and T. F. Heinz, *Nano Letters* **16**, 4831 (2016).
- <sup>53</sup> Z. Y. Zhu, Y. C. Cheng, and U. Schwingenschlögl, *Phys. Rev. B* **84**, 153402 (2011).
- <sup>54</sup> D. Xiao, G.-B. Liu, W. Feng, X. Xu, and W. Yao, *Phys. Rev. Lett.* **108**, 196802 (2012).
- <sup>55</sup> E. Suárez Morell, J. D. Correa, P. Vargas, M. Pacheco, and Z. Barticevic, *Phys. Rev. B* **82**, 121407 (2010).
- <sup>56</sup> A. O. Sboychakov, A. L. Rakhmanov, A. V. Rozhkov, and F. Nori, *Phys. Rev. B* **92**, 075402 (2015).
- <sup>57</sup> L. A. Gonzalez-Arraga, J. L. Lado, F. Guinea, and P. San-Jose, *Phys. Rev. Lett.* **119**, 107201 (2017).
- <sup>58</sup> C. L. Kane and E. J. Mele, *Phys. Rev. Lett.* **95**, 226801 (2005).
- <sup>59</sup> H. Rostami, A. G. Moghaddam, and R. Asgari, *Phys. Rev. B* **88**, 085440 (2013).
- <sup>60</sup> H. Shi, H. Pan, Y.-W. Zhang, and B. I. Yakobson, *Phys. Rev. B* **87**, 155304 (2013).
- <sup>61</sup> P. San-Jose and E. Prada, *Phys. Rev. B* **88**, 121408 (2013).
- <sup>62</sup> R. Bistritzer and A. H. MacDonald, *Proceedings of the National Academy of Sciences* **108**, 12233 (2011).
- <sup>63</sup> K.-T. Chen and P. A. Lee, *Phys. Rev. B* **84**, 205137 (2011).
- <sup>64</sup> A. L. R. Manesco, J. L. Lado, E. V. Ribeiro, G. Weber, and J. Rodrigues, Durval, arXiv e-prints , arXiv:2003.05163 (2020), arXiv:2003.05163 [cond-mat.mes-hall].
- <sup>65</sup> T. M. R. Wolf, J. L. Lado, G. Blatter, and O. Zilberberg, *Phys. Rev. Lett.* **123**, 096802 (2019).
- <sup>66</sup> A. Lopez-Bezanilla and J. L. Lado, arXiv e-prints , arXiv:2005.02169 (2020), arXiv:2005.02169 [cond-mat.mes-hall].
- <sup>67</sup> E. Colomés and M. Franz, *Phys. Rev. Lett.* **120**, 086603 (2018).
- <sup>68</sup> A. Ramires and J. L. Lado, *Phys. Rev. Lett.* **121**, 146801 (2018).
- <sup>69</sup> A. Ramires and J. L. Lado, *Phys. Rev. B* **99**, 245118 (2019).
- <sup>70</sup> C. Xu and L. Balents, *Phys. Rev. Lett.* **121**, 087001 (2018).
- <sup>71</sup> M. Koshino, N. F. Q. Yuan, T. Koretsune, M. Ochi, K. Kuroki, and L. Fu, *Phys. Rev. X* **8**, 031087 (2018).
- <sup>72</sup> J. Kang and O. Vafek, *Phys. Rev. X* **8**, 031088 (2018).
- <sup>73</sup> J. a. E. H. Braz, B. Amorim, and E. V. Castro, *Phys. Rev. B* **98**, 161406 (2018).
- <sup>74</sup> D. R. Klein, D. MacNeill, J. L. Lado, D. Soriano, E. Navarro-Moratalla, K. Watanabe, T. Taniguchi, S. Manni, P. Canfield, J. Fernández-Rossier, and P. Jarillo-Herrero, *Science* **360**, 1218 (2018).
- <sup>75</sup> C. Cardoso, D. Soriano, N. A. García-Martínez, and J. Fernández-Rossier, *Phys. Rev. Lett.* **121**, 067701 (2018).
- <sup>76</sup> J. Zhou, J. Qiao, C.-G. Duan, A. Bournel, K. L. Wang, and W. Zhao, *ACS Applied Materials & Interfaces* **11**, 17647 (2019).
- <sup>77</sup> S. Mashhadi, Y. Kim, J. Kim, D. Weber, T. Taniguchi, K. Watanabe, N. Park, B. Lotsch, J. H. Smet, M. Burghard, and K. Kern, *Nano Letters* **19**, 4659 (2019).
- <sup>78</sup> K. Zollner, P. E. Faria Junior, and J. Fabian, *Phys. Rev. B* **100**, 085128 (2019).
- <sup>79</sup> “The elk code, <http://elk.sourceforge.net/>,” .
- <sup>80</sup> F. Bultmark, F. Cricchio, O. Grånäs, and L. Nordström, *Phys. Rev. B* **80**, 035121 (2009).
- <sup>81</sup> G. Catarina, N. M. R. Peres, and J. Fernández-Rossier, *2D Materials* **7**, 025011 (2020).
- <sup>82</sup> L. Ciorciaro, M. Kroner, K. Watanabe, T. Taniguchi, and A. Imamoglu, *Phys. Rev. Lett.* **124**, 197401 (2020).
- <sup>83</sup> T. P. Lyons, D. Gillard, A. Molina-Sánchez, A. Misra, F. Withers, P. S. Keatley, A. Kozikov, T. Taniguchi, K. Watanabe, K. S. Novoselov, J. Fernández-Rossier, and A. I. Tartakovskii, arXiv e-prints , arXiv:2004.04073 (2020), arXiv:2004.04073 [cond-mat.mes-hall].